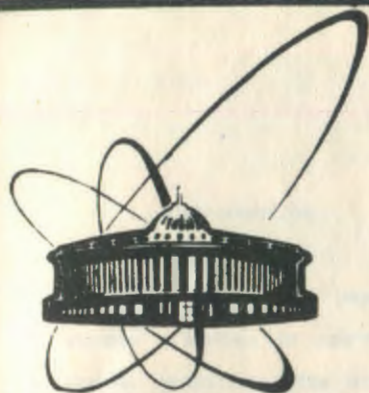


90-177



ОБЪЕДИНЕННЫЙ
ИНСТИТУТ
ЯДЕРНЫХ
ИССЛЕДОВАНИЙ
ДУБНА

B 17

E11-90-177

N.S. Bakhvalov ¹, G.S. Kazacha, K.K. Likharev ¹,
S.I. Serdyukova

STATICS AND DYNAMICS OF SINGLE-ELECTRON
SOLITONS IN TWO-DIMENSIONAL ARRAYS
OF ULTRASMALL TUNNEL JUNCTIONS

Submitted to "Physica B"

¹Moscow State University, Moscow 119899 GSP, USSR

1990

1. INTRODUCTION

In our previous paper [1] we have analyzed the electric charge transfer in one-dimensional arrays of very-small-area tunnel junctions. The statics and dynamics of the charge has been shown to be most adequately described in terms of single-electron ($\pm e$ -charged) topological solitons which can be injected into the array and driven along it by the external electric field. Under certain conditions, the soliton motion can be virtually periodic in time with the frequency $f_s = I/e$, where I is the average (dc) current flowing along the array due to the soliton motion. (Such "Single-Electron-Tunneling" (SET) oscillations had been predicted earlier to take place in single current-biased junctions - see Ref. [2] for a recent review). This prediction has been confirmed in recent experiments [3] with one-dimensional arrays of Al/Al-oxide/Al tunnel junctions of area below $0.01 \mu^2$ at millikelvin temperatures.

Present-day nanolithographic technologies enable one to fabricate not only one-dimensional, but also two-dimensional quasi-uniform arrays of the ultrasmall junctions [4-6]. This is why an extension of the concept of the single-electron solitons to the two-dimensional case is of a considerable interest for both theory and experiment. Such an extension is a subject of the present work. Our results for measurable properties of the arrays are compared with those of the recent Ref. [7] where the concept was not employed explicitly.

2. ARRAY MODEL AND BASIC RELATIONS

Consider a uniform rectangular two-dimensional array of $N \times M + (N-1) \times (M-1)$ tunnel junctions formed between $N_{\text{tot}} = (N-1) \times M$ normal-metal "islands" (Fig. 1a). Just as in Ref. [1], we will take into account the junction capacitances C as well as intrinsic ("stray") capacitances C_0 of the electrodes, but will neglect mutual capacitances C_{ij} between non-adjacent islands (Fig. 1b). Strictly speaking, such a model is only valid for the arrays placed close to a common "ground plane" conductor; it can nevertheless serve as a reasonable approximation to real experimental structures [3-6].

An external electric voltage $V = V_+ - V_-$ across the array is fixed by potentials of two edge electrodes (Fig. 1a); note that the independent combination of the potentials, $U = (V_+ + V_-)/2$, is of an importance as well, because it fixes the average potential of the array (referred to the common ground) [1].

As an evident generalization of the one-dimensional structure [1], the two-dimensional array is described by the following free (Gibbs) energy

$$\begin{aligned} \mathcal{G} = & \sum_{n=1}^{N-1} \sum_{m=1}^{M-1} \frac{Q_{n,m}^2}{2C_0} + \sum_{n=1}^N \sum_{m=1}^M \frac{C}{2} (\phi_{n,m} - \phi_{n-1,m})^2 \\ & + \sum_{n=1}^{N-1} \sum_{m=1}^{M-1} \frac{C}{2} (\phi_{n,m} - \phi_{n,m+1})^2 - \sum_{m=1}^M (V_- q_{-,m} + V_+ q_{+,m}). \end{aligned} \quad (1)$$

Here $Q_{n,m}$ and $\phi_{n,m}$ are electric charges and potentials of the metallic islands (for numeration, see Fig. 1), while

$$q_{-,m} \equiv ek_{-,m} + C(V_- - \phi_{-,m}), \quad q_{+,m} \equiv ek_{+,m} + C(V_+ - \phi_{+,m}), \quad (2)$$

where $k_{-,m}$ ($k_{+,m}$) are numbers of electrons injected into islands of the left (right) row from the edge electrodes.

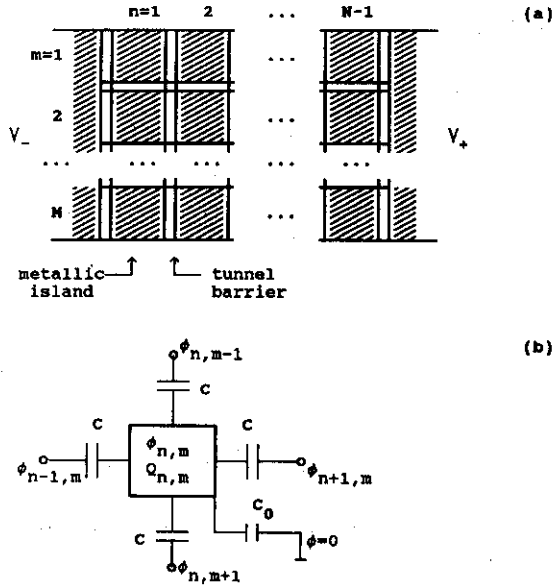


Fig. 1. Two-dimensional array of tunnel junctions: (a) general scheme of the array and our way of numeration of its metallic islands and (b) equivalent circuit of an internal island accepted in this work (islands of the lateral rows ($m=1, M$) lack one of the junction capacitances C).

Continuity of the electric charge yields the following equations relating the charges and potentials:

$$\begin{aligned}
 & -C [\phi_{n-1,m} + \phi_{n+1,m} + (1-\delta_{m,1})\phi_{n,m-1} + (1-\delta_{m,M})\phi_{n,m+1}] \\
 & + [C_0 + C(4-\delta_{m,1}-\delta_{m,M})]\phi_{n,m} = Q_{n,m}, \quad \text{for } 1 \leq n \leq N-1, 1 \leq m \leq M, \quad (3)
 \end{aligned}$$

where $\phi_{0,m} \equiv V_-$, $\phi_{N,m} \equiv V_+$.

Provided the tunnel conductances G of the junctions are low enough,

$$G \ll e^2/h, \quad (4)$$

the single electron tunneling rate through a junction can be calculated from a simple formula [2]

$$\Gamma = \frac{G}{e} F\left(-\frac{\Delta\mathcal{G}}{e}\right), \quad F(x) = x/[1-\exp(-ex/k_B T)], \quad (5)$$

where $\Delta\mathcal{G}$ is a change of the Gibbs energy \mathcal{G} (1) in the result of the tunneling event. It is easy to check [8] that the change resulting from the tunneling of an electron from island (n,m) to island (n',m') can be presented in a simple form (cf. eq. (6) of Ref. 1)

$$\Delta\mathcal{G} \equiv \mathcal{G}' - \mathcal{G} = \frac{e}{2} (\phi_{n,m} + \phi'_{n,m} - \phi_{n',m'} - \phi'_{n',m'}), \quad (6)$$

where (') denotes values after the tunneling event. In particular,

$$Q'_{n,m} = Q_{n,m} - e, \quad Q'_{n',m'} = Q_{n',m'} + e, \quad (7)$$

so that Eqs. (3), (5)-(7) form a complete system of (stochastic) equations which allows one to analyze statics and dynamics of the array [1].

Before we start the analysis let us note that an arbitrary solution of Eq. (3) can be expressed explicitly as follows [8]:

$$f_{n,m} = K_-(n) V_- + K_+(n) V_+ + \sum_{k=-(M-1)}^{M-1} L_k(n, n_0) T_k(m, m_0) F Q_{n_0, m_0} \quad (8)$$

Here functions K_- and K_+ coincide with those for the one-dimensional case ($M=1$):

$$K_+(n) = \frac{1}{1-k_0^{2N}} [k_0^{N-n} - k_0^{n+N}], \quad K_-(n) = \frac{1}{1-k_0^{2N}} [k_0^n - k_0^{2N-n}], \quad (9)$$

the traversal Green functions are very simple:

$$T_k(m, m_0) = \cos[p_M^k(m - \frac{1}{2})] \cos[p_M^k(m_0 - \frac{1}{2})], \quad (10)$$

while the longitudinal Green functions are similar to those for the one-dimensional case:

$$L_k(n, n_0) = \frac{1}{MC_k} (k_k^{1n-n_0} - \frac{k_k^{N-n_0} k_k^{n_0-N} k_k^n + [k_k^{n_0-k_k} k_k^{-n_0} k_k^{N-n}]}{k_k^N - k_k^{-N}}), \quad (11)$$

but with a specific characteristic number k_k and effective capacitance C'_k for each traversal Fourier mode:

$$k_k = \exp(-l_k) = 1 + \frac{C_{0k}}{2C} - \left[\left(\frac{C_{0k}}{2C} \right)^2 + \frac{C_{0k}}{C} \right]^{1/2}, \quad (12)$$

$$C'_k = [C_{0k}^2 + 4CC_{0k}]^{1/2}, \quad C_{0k} = C_0 + 4C \sin^2 \frac{pk}{2M}. \quad (13)$$

The solution expressed by Eqs.(8)-(13) will be quite useful for some further calculations.

3. TWO-DIMENSIONAL SINGLE-ELECTRON SOLITONS

Consider a large array ($M, N \gg 1$) with only one electron (or hole) injected into an island far enough of all the array edges:

$$Q_{n,m}^{(s)} = \pm e \delta_{n,n_0} \delta_{m,m_0}. \quad (14)$$

According to Eq. (3), it produces a nearly axial-symmetric distribution of the potential (Fig. 2b) approaching zero far from the central point (n_0, m_0) :

$$\phi_{n,m}^{(s)} = \frac{\pm e}{2\sqrt{\pi} (CC'_0)^{1/2}} \frac{\kappa_0^r}{\sqrt{r}}, \quad \text{for } r = [(n-n_0)^2 + (m-m_0)^2]^{1/2} \gg 1 \quad (15)$$

(close to the center the symmetry is distorted by the array discreteness). This is essentially the two-dimensional single-electron topological soliton (or antisoliton) which forms as a result of a mutual polarization of the adjacent metallic islands (Fig. 2a, to be compared Fig. 2b of Ref. [1]).

Energy E of the soliton is fundamentally related as $E = e\phi_0/2$ to the electric potential value $\phi_0 = \phi_{n_0, m_0}$ in its center, and can be readily found from the general Eqs. (8)-(13). Figure 3 shows E (and hence ϕ_0) as a function of the only dimensionless parameter of the problem, the ratio C_0/C .

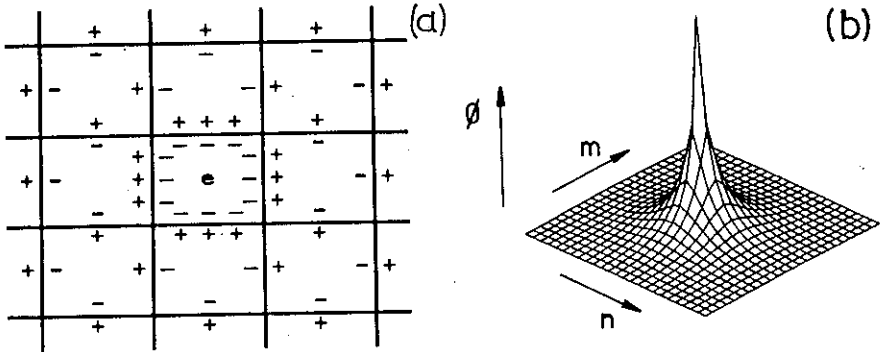


Fig. 2. Single-electron soliton placed into the two-dimensional array far enough of its edges: (a) schematic structure of the electric charge distribution and (b) map of the island potentials for $C_0/C=0.1$.

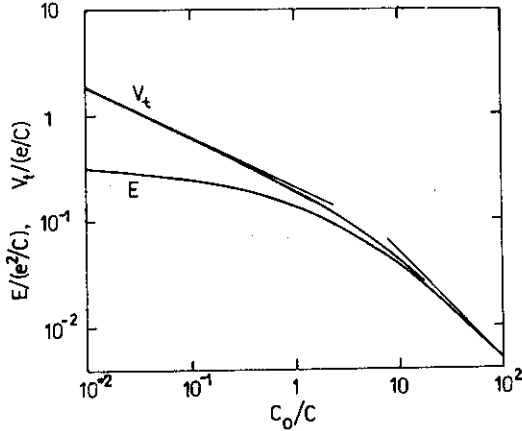


Fig. 3. Energy E (and hence the maximum potential $|\phi_0|=2E/e$) of the two-dimensional soliton, and the voltage threshold V_t for the soliton entrance into a large ($N, M \gg 1, \lambda_0^{-1}$) array as functions of the stray capacitance C_0 . Thin lines correspond to asymptotic expressions (16), (20).

The following asymptotic expressions are important:

$$E = \frac{e^2}{2C_0} \times \begin{cases} \frac{C_0}{4\pi C} \ln\left(\frac{32C}{C_0}\right), & \text{for } C_0 \ll C, \\ 1, & \text{for } C_0 \gg C; \end{cases} \quad (16)$$

note that in the former (most important) limit the energy is much less than that of the one-dimensional soliton [1].

According to Eq. (6), energy of interaction of the soliton with any fixed external field $\phi_{n,m}^{(e)}$ (say, a field $\phi_{n,m}^{(s)}$ induced by another soliton) can be presented just as

$$U(s-s) = \pm e \phi_{n_0, m_0}^{(s)}. \quad (17)$$

According to Eq. (15), the soliton-soliton interaction scales as $r^{-1/2}$ at medium distances r between their centers ($1 \ll r \ll \lambda_0^{-1}$) and is cut off exponentially at $r \gg \lambda_0^{-1}$. Sign of the interaction corresponds, as usual, to repulsion of the solitons of the same polarity and to attraction between a soliton and an antisoliton.

Soliton interaction with a "passive" (unbiased) edge electrode can be described by its mirror reflection in the boundary plane ($n=0$ or $n=N$ in Fig. 1), with change of polarity to the opposite one:

$$U(s-ee) = -e \times \begin{cases} |\phi_{-n_0, m_0}^{(s)}|, & \text{for left electrode,} \\ |\phi_{2N-n_0, m_0}^{(s)}|, & \text{for right electrode,} \end{cases} \quad (18)$$

so that the boundary attracts the soliton of any polarity. On the contrary, the lateral edge of the array *repulses* any soliton just as its mirror reflection in the planes $m=1/2$ or $m=M+1/2$, of the same polarity:

$$U(s-le) = e \times \begin{cases} |\phi_{n_0, -m_0+1}^{(s)}|, & \text{for upper edge,} \\ |\phi_{n_0, 2M-m_0+1}^{(s)}|, & \text{for lower edge.} \end{cases} \quad (19)$$

(Note that it is essentially the latter reflection symmetry which makes the traversal Fourier expansion (8)-(10) possible;

the former (anti)symmetry (18) allows also an alternative (longitudinal) Fourier expansion of any potential distribution, with the basic functions $\sin(\pi k'n/N)$, where $1 \leq k' \leq N$.)

Finally, the soliton interacts also with potentials $\phi_{\pm}^{(e)}$ induced by external voltages V_{\pm} ; this interaction can be described by a formula similar to Eq. (17). Combining this formula with Eqs. (18), (19) one can readily calculate the threshold value V_t of the voltage necessary to inject the solitons into the array, and thus to overcome its "Coulomb blockade" state [1,2]. Due to the soliton repulsion from the lateral edges, the threshold is lowest for the middle rows ($m \approx M/2$); for an array large enough ($N, M \gg 1$, λ_0^{-1}) one obtains

$$V_t = \frac{e}{2C_0} \times \begin{cases} (1 - \frac{2}{\pi}) \times (\frac{C_0}{C})^{1/2}, & \text{for } C_0 \ll C, \\ 1, & \text{for } C_0 \gg C. \end{cases} \quad (20)$$

Figure 3 shows V_t for intermediate values of the ratio C_0/C .

Formula (20) shows that in the most important case $C_0/C \ll 1$ the Coulomb blockade threshold is a factor of ~ 3 less than that in a similar one-dimensional array (see Eq. (16) of Ref. [1]). This formula is in an order-of-magnitude accord with the value $V_t \approx 0.5$ mV observed [5,6] in high-ohmic arrays of 190×60 Al/Al-oxide/Al junctions with estimated parameters $C \sim 3 \times 10^{-16}$ F and $C_0 \sim 10^{-16}$ F, although a more quantitative comparison would require an independent measurement of these parameters.

4. STATICS

If the external electrode potentials V_{\pm} are close to each other, so that $V \approx 0$, their increase beyond the threshold V_t leads to formation of a static pattern of the single-electron solitons in the array. Mutual repulsion of the solitons tries

to order them to form a regular lattice (the two-dimensional Wigner crystal), while intrinsic periodicity of the junction array ($\Delta N=1$, $\Delta M=1$) distorts the crystal until their periods are commensurate. Figure 4c shows an example of the consequence of the soliton configurations for a gradual increase of the external potential U . Note that at $U \approx V_t$ the solitons prefer the middle rows of the array due to their repulsion from its lateral edges, described by Eq. (19).

Another important fact is that the consequent configurations differ (as a rule) by more than one soliton move. It means that the configurations are separated by intermediate ones, with larger energies. This is why each real configuration is (locally) stable and holds on within some range of U (one can speak about pinning of a particular soliton pattern by the array).

As a result, the total number n of solitons is a hysteretic function of U , consisting of horizontal steps with $\Delta n=1$ (Fig. 4a). Comparison of this pattern for a wide array ($M - N \gg 1$) with that (Fig. 4b) for the one-dimensional array ($M=1$) with the same total number of islands and the same ratio C_0/C shows that the former pattern is somewhat less hysteretic. It means that in the two-dimensional case the Wigner crystal pinning is weaker, apparently because of a larger number of topological ways between the adjacent stable configurations.

5. DYNAMICS

The last fact is very important for drift of the solitons, which can be induced by a sufficiently large "transport" voltage $V=V_- - V_+$ [1]. Really, if the pinning is small, the Wigner crystal can move along the array without

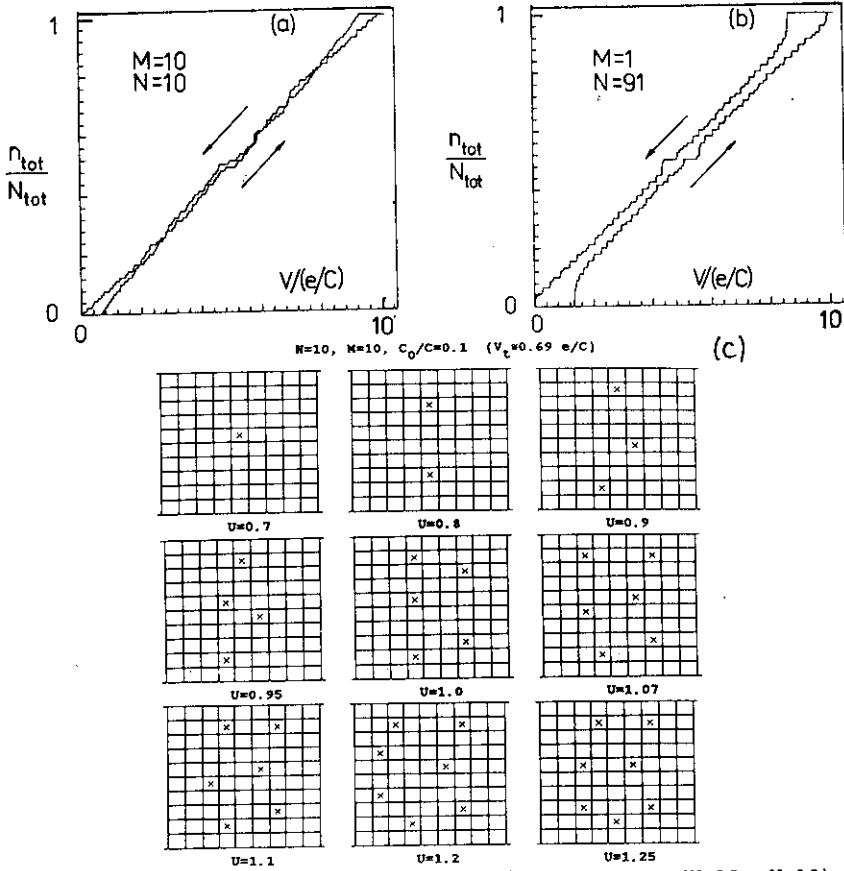


Fig. 4. Filling of the 9×10 -island array ($N=10, M=10$) with $C_0/C=0.1$ by solitons at $V_-=V_+=U$: (c) several first successive configurations forming as U is increased (solitons are denoted by crosses); (a) total number n_{tot} of the solitons in the array as a function of U for increasing and decreasing field; (b) the similar function for a one-dimensional array with the same C_0/C ratio and total number of islands $N_{tot} = M \times (N-1) = 90$ ($N=91, M=1$). Each step of the pattern corresponds to $\Delta n_{tot} = 1$; for further values of U , the pattern is reproduced translationally with periods $\Delta n = N_{tot}$ and $\Delta U = e/C_0$. Here and below, temperature has been supposed to be low enough ($k_B T \ll e^2/2C$).

melting, so that the space order (correlation) of the solitons gives rise to the time order (coherence) of the electrons entering and leaving the array through the external electrodes. If the coherence were complete, the process would be completely periodic in time, with the frequency [1,2]

$$f_s = I/e, \quad (21)$$

where I is the average (dc) current carried by the solitons. In practice, the coherence is never perfect, so that the "SET" oscillations (21) have a nonvanishing linewidth.

In order to calculate dynamic characteristics of the two-dimensional arrays, we have used the same Monte-Carlo method as for the one-dimensional structures [1] (with some acceleration of the frequency spectrum calculation procedure, kindly suggested by A. Korotkov). Note that for this purpose we use in particular Eq. (5) with energy \mathcal{E} of the whole array rather than some local part of it. This approach corresponds to what the authors of Ref. [7] call the global rule; in accordance with recent theoretical [9] and experimental [10] results we believe that this case alone is real for the present-day experimental structures.

Figure 5 shows typical dc I-V curves of relatively long arrays ($N=21$) of various widths, and frequency spectra of the charge

$$Q_- = \sum_{m=1}^M C(V_- - \phi_{1,m}) \quad (22)$$

of the left electrode (results for another electrode are similar) calculated for a one value of I [11]. One can see that increase of the width leads to a gradual decrease of the Coulomb blockade range ($I=0$, $|V| < V_t$), in accordance with Eq. (20). The general shape of the I-V curves is qualitatively close to that of the one-dimensional arrays. As the current increases, the curve gradually approaches the linear asymptote

$$I = \frac{G}{N} M (V - V_{\text{Of}} \times \text{sign } V); \quad (23)$$

magnitude of the "voltage offset" V_{Of} is discussed in Appendix.

Figure 5b shows that linewidth of the SET oscillations grows with M . This qualitative conclusion is in accordance with that made by Geigenmüller and Schön [7], despite a significant difference of the spectrum shapes (due to the different bias type, see Sec. 4). Nevertheless, longer arrays with smaller C_0/C do exhibit some reduction of the linewidth when their width is increased from one to few junctions, at very small oscillation frequencies. For example, linewidth of oscillations with $f_s = 0.005$ eG/C in a 32-junction-long array with $C_0/C = 0.01$ is reduced from ~60% to only 15% of f_s by increase of the array width M from 1 to 5 (a further increase again results in the line broadening).

We believe that the reason of this behavior is as follows. If V is beyond but very close to V_t , the solitons enter and move along only one (central) row of the array, because of their repulsion from its lateral edges, so that the array dynamics is very close to that of the one-dimensional arrays. For the latter system of a fixed length $N \gg 1$, there exists an optimum value of C_0/C providing the smallest linewidth at a given frequency f_s (this value provides an optimum size λ_0^{-1} of the solitons and hence an optimum degree of their repulsion, so that the number of the solitons moving simultaneously along the array is close to the optimum value 2-3). According to Eqs. (8)-(13) the two-dimensionality of the array ($M > 1$) reduces the effective size of the solitons, and hence can bring it either closer to or farther from the optimum value. Note again that the former case is realized only for very low frequencies, large N , and small C_0/C .

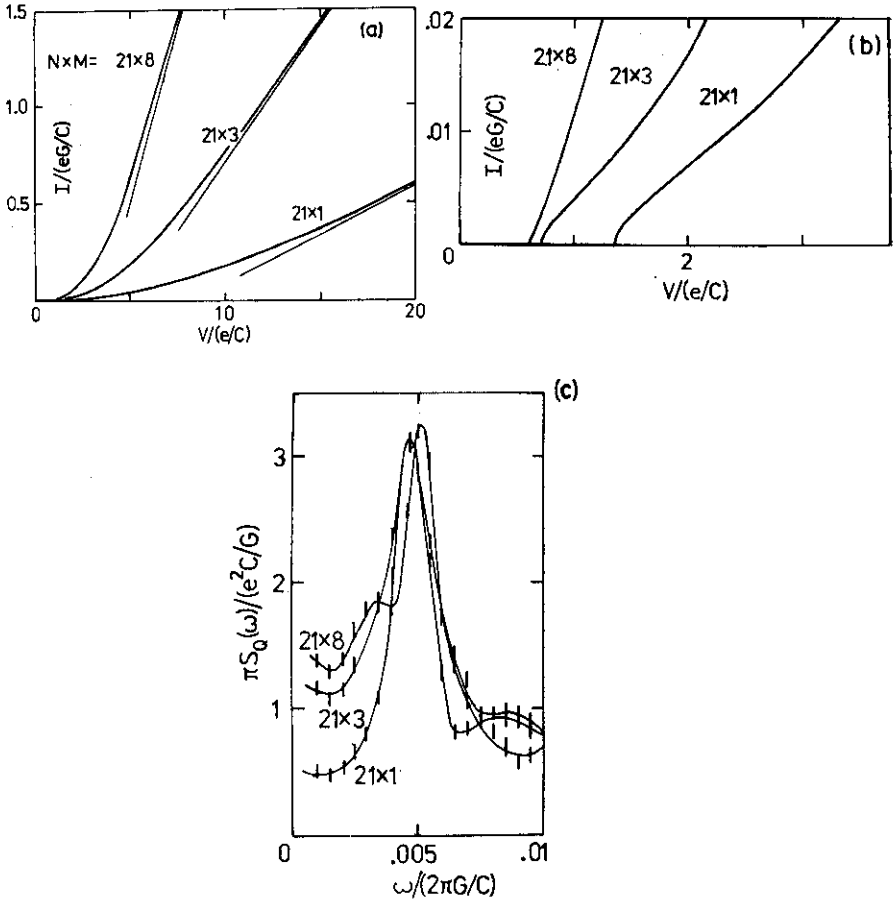


Fig. 5. (a) Global shape of the dc I-V curves, (b) blow-up of their low-current parts and (c) frequency spectra of the electrode charge for three arrays with equal length ($N=21$), parameter C_0 ($C_0/C=0.1$), dc current ($I=0.005$ eG/C), and similar boundary conditions ($V_- = V$, $V_+ = 0$), but various widths ($M=1, 3$, and 8). Thin lines in Fig. 5a show the asymptotes (23). Error bars in Fig. 5c show the accuracy provided by our numerical simulation of the array dynamics; thin lines are only guides for the eye.

At larger $V-V_t$ (and hence larger I and f_g), the solitons enter other rows of the array as well, so that the Wigner crystal formed by them becomes two-dimensional itself, and all its rows give their own contributions to the SET oscillation waveform. Now, even small pinning leads to random phase shifts between the soliton lines in far rows (i.e., to destruction of the long range order of the Wigner crystal) and as a consequence to suppression of the coherence of the SET oscillations.

6. CONCLUSION

We have found that the concept of the single-electron solitons, developed earlier for one-dimensional arrays of ultrasmall tunnel junctions, is equally useful for description of the correlated tunneling in two-dimensional arrays. In particular, the concept allows a ready calculation of the threshold of the Coulomb blockade and of the dc voltage offset of the I-V curve asymptotes, and provides a visual interpretation of all the basic static and dynamic properties of the arrays revealed by the numerical calculations.

ACKNOWLEDGEMENTS

Useful discussions with D. Averin, U. Geigenmüller, A. Korotkov, J. Madjarova, G. Schön, A. Ustinov, and A. Zorin are gratefully acknowledged.

APPENDIX

Voltage Offset in 1-D and 2-D Arrays

Consider a uniform array biased with a large voltage:

$$eV/N \gg e^2/C, k_B T. \quad (\text{A.1})$$

This condition allows one to neglect the backward tunneling of the electron. Then according to Eq. (5) the average current between n-th and (n+1)-th islands of some row can be expressed as

$$I_m = -e\Gamma = (G/e) \Delta\mathcal{S}. \quad (\text{A.2})$$

Let us denote the matrix reciprocal to that of the linear system of equations (3) as $\|C^{-1}\|$. Then Eq. (6) yields

$$\Delta\mathcal{S} = e(\phi_{n+1} - \phi_n) + \frac{e^2}{2} [(C^{-1})_{n,n} - 2(C^{-1})_{n,n+1} + (C^{-1})_{n+1,n+1}], \quad (\text{A.3})$$

where we have omitted indices $m=m'$. Now, let us neglect the electron transfer between the rows of the array (numerical simulations show that this process is really vanishing at $V \rightarrow \infty$). Then I_m does not depend on n, and summation of Eq. (A.3) over this index yields an expression similar to Eq. (23) with

$$V_{of} = e \sum_{n=1}^{N-1} [(C^{-1})_{n,n} - (C^{-1})_{n,n+1}] \quad (\text{A.4})$$

(the second term is in fact vanishing for $n=N-1$).

Equations (A.3) and (A.4) are very similar in structure to Eq. (8) of Ref. [7], but nevertheless do differ from it. We believe that the main origin of this difference is that the authors of Ref. [7] have neglected a dependence of the voltage drop $V_n = \phi_{n+1} - \phi_n$ on the junction number in the row (according to Eq. (A.3), this dependence is quite substantial). They have also implicitly averaged V_{of} over the rows. Equation (A.4) shows, however, that in a genuinely two-dimensional array ($N, M \gg 1$, λ_0^{-1}) the offset can be dependent of the row number:

$$V_{of} = \frac{e}{C} \times \left\{ \begin{array}{ll} \frac{N}{4} - \frac{1}{4\sqrt{2}}, & \text{for } m=M/2, \\ \frac{N}{\pi} + \frac{1}{2} - \frac{1}{\sqrt{2}}, & \text{for } m=1, M, \end{array} \right\} \text{ for } C_0 \ll C, \quad (\text{A.5})$$

$$\left(\frac{C}{(N-1)C_0} \right) \text{ for all } m, \text{ for } C_0 \gg C.$$

This dependence (confirmed reliably by our numerical simulations) means that even in the limit $V \rightarrow \infty$ the current is not distributed uniformly across the array width, but is suppressed slightly in its edge rows ($m \approx 1, M$), due to the soliton repulsion by the lateral edges. The offset averaged over the rows is nevertheless close to that calculated (for the limit $C_0 = 0$) in Ref. [7].

Equation (A.4) is of course valid for one-dimensional arrays ($M=1$) as well, and for a long array ($N \gg 1, \lambda_0^{-1}$) it yields

$$V_{\text{of}} = \frac{e}{c} \times \begin{cases} \frac{N}{2} \left(1 - \frac{\lambda_0}{2}\right), & \text{for } C_0 \ll C, \\ (N-1) \frac{c}{C_0 + 3C}, & \text{for } C_0 \gg C. \end{cases} \quad (\text{A.6})$$

Note a difference between the first of these equations and Eq. (2) of Ref. [12]; this difference is, however, negligible for the practical arrays discussed in the cited work.

REFERENCES

- [1] N.S. Bakhvalov, G.S. Kazacha, K.K. Likharev, and S.I. Serdyukova, Zh. Eksp. Teor. Fiz. 95 (1989) 1010 [Sov. Phys. - JETP 68 (1989) 581]; IEEE Trans. Magn. 25 (1989) 1436.
- [2] D.V. Averin and K.K. Likharev, in: "Quantum Effects in Small Disordered Systems", ed. by B. Al'tshuler et al. (Elsevier, Amsterdam, to be published).
- [3] P. Delsing, K.K. Likharev, L.S. Kuzmin, and T. Claeson, Phys. Rev. Lett. 63 (1989) 1861.
- [4] L.J. Geerligs, V.F. Anderegg, C.A. van der Jeugd, J. Romijn, and J.E. Mooij, Europhys. Lett. 10 (1989) 79.
- [5] L.J. Geerligs and J.E. Mooij, Physica B 152 (1989) 207.
- [6] L.J. Geerligs, M. Peters, L.E.M. de Groot, A. Verbruggen, and J.E. Mooij, Phys. Rev. Lett. 63 (1989) 326.

- [7] U. Geigenmüller and G. Schön. *Europhys. Lett.* 10 (1989) 765.
- [8] G.S. Kazacha, J.D. Madjarova, and S.I. Serdyukova, Preprint No. P11-89-703 (Joint Inst. Nucl. Res., Dubna, 1989).
- [9] Yu.V. Nazarov, *Zh. Eksp. Teor. Fyz.* 95 (1989) 975 [*Sov. Phys. - JETP* 68 (1989) 561].
- [10] P. Delsing, K.K. Likharev, L.S. Kuzmin, and T. Claeson, *Phys. Rev. Lett.* 63 (1989) 1180.
- [11] These our results are qualitatively similar to but quantitatively different from those obtained in Ref. [7] (for the "global rule"). Possibly the difference is due to our assumption of fixed voltage across the array (this assumption is apparently adequate to real experiments [1,2]) rather than that of fixed current accepted in Ref. [7].
- [12] L.S. Kuzmin, P. Delsing, T. Claeson, and K.K. Likharev, *Phys. Rev. Lett.* 62 (1989) 2539.

Received by Publishing Department
on March 12, 1990.